

Combined Effect of Long Processing Time and Na_2SiF_6 on the Properties of PEO Coatings Formed on AZ91D

Zeeshan Ur Rehman and Bon Heun Koo

(Submitted October 24, 2015; in revised form May 23, 2016; published online June 17, 2016)

In this study, protective ceramic coatings were prepared on AZ91D magnesium alloy by plasma electrolytic oxidation (PEO) to improve the corrosion and mechanical properties of AZ91D magnesium alloy. The process was conducted in silicate-fluoride-based electrolyte solution. It was found that the average micro-hardness of the coating was significantly increased with an increase in the PEO processing time. The highest value of the average micro-hardness ~ 1271.2 HV was recorded for 60-min processing time. The phase analysis of the coatings indicated that they were mainly composed of Mg_2SiO_4 , MgO, and MgF_2 phases. The surface and cross-sectional study demonstrated that porosity was largely reduced with processing time, together with the change in pore geometry from irregular to spherical shape. The results of the polarization test in 3.5 wt.% NaCl solution revealed that aggressive corrosion took place for 5-min sample; however, the corrosion current was noticeably decreased to 0.43×10^{-7} A/cm² for the 60-min-coated sample. The superior nobility and hardness for long processing time are suggested to be due to the dense and highly thick coating, coupled with the presence of MgF_2 phase.

Keywords AZ91D, corrosion, hardness, microstructure, Na_2SiF_6 , PEO

1. Introduction

The global demand of magnesium and its alloys are increasing day by day due to their attractive properties such as low density, high strength/weight ratio, high-dimensional stability, high damping capacity, and suitability for recycling (Ref 1-7). However, the poor corrosion resistance of Mg alloys limits their use in many various applications, especially in corrosive environments (Ref 8-10). To cope with the corrosion vulnerability of magnesium alloys, several coating processes have been developed, e.g., conversion coating, electrochemical plating, and anodizing and plasma electrolytic oxidation (PEO) (Ref 11-13).

Out of all these coating methods, PEO has proved to be an environment friendly and inexpensive method to form a thick, hard, and adherent ceramic coating on the surface of Mg, Al, and Ti alloys (Ref 14-18). Researchers unanimously considered PEO as a very effective technique to improve the corrosion and wear resistance of magnesium and magnesium alloys (Ref 15, 18-21). In the PEO process, ions species from the electrolyte solution are deposited in the form of a layer on an alloy substrate due to high temperature discharge plasma, generated by applying an extremely high anodic potential in a specific electrolyte (Ref 15, 22). The properties of the oxide layer produced by the PEO process depend on various processing conditions, including chemical composition, processing time,

applied bias, substrate composition, and post-annealing treatment (Ref 23-29).

Like the other PEO process parameters, processing time is also a very important parameter in terms of both experimental and commercial aspects. It significantly influences the cost of the operation, if properly optimized. Therefore, optimization and effect of processing time together with other process parameters on various properties of PEO coatings has been studied by various authors (Ref 23-26, 29). However, the influence of long processing time in silicate-fluoride-based electrolyte solution has never been studied before. The present study is therefore devoted to examine the effect of processing time on various properties of PEO coatings produced on AZ91D in silicate-fluoride-based electrolyte solution.

2. Experimental Method

2.1 Specimen and Coating Process

Commercial AZ91D (Al 9.1, Zn 0.85 Mn 0.27, Fe \leq 0.02, others \leq 0.01, Mg balance all in wt.%) coupons with 13 mm diameter and 5.9 mm thickness were used in this study. Before the PEO process, samples were polished with SiC paper (up to grade 2000) followed by decreasing in deionized water and ethanol. The final surface roughness for the sample was found to be in the range of 0.1 ± 0.05 μm .

The PEO process was conducted by means of external power supply with maximum power of 20 kW, under hybrid voltage source of 200AC and 260DC volts. Hybrid voltage sources were used to achieve thick and hard coating. The current was allowed to vary while the AC and DC voltages were kept constant through all the experiment. The electrolyte used was consisted of 12 g/L sodium silicate (Na_2SiO_3), 3 g/L sodium hydroxide (NaOH), and 0.3 g/L Na_2SiF_6 . Temperature of the electrolyte was maintained below 25 °C during the process by adjusting the cool water circulation. Coatings on AZ91D alloy were produced for 5-, 15-, 30-, and 60-min

Zeeshan Ur Rehman and Bon Heun Koo, School of Materials Science and Engineering, Changwon National University, Changwon 641-773, South Korea. Contact e-mail: bhkoo@changwon.ac.kr.

processing time as mentioned in Table 2. After PEO treatment, the coated samples were rinsed with deionized water and dried in the air.

2.2 Phase Composition and Microstructure

The phase composition of the coating was investigated by means of x-ray diffraction (XRD), using a Cu K_{α} source in the range of 20° to 80° . The microstructure of the coated samples was observed under scanning electron microscope (SEM).

For the cross section observation, the coated samples were cut and cross sections of the samples were polished down to $0.1\ \mu\text{m}$ for SEM examination. A thin layer of gold was sputtered over the polished surface of cross section to ensure adequate electrical conductivity during SEM observation. Average thickness and porosity was calculated for each sample using imageJ software.

2.3 Hardness and Electrochemical Tests

Vickers hardness of the polished cross sections of the coating layers was measured on 10 different places by a VLPK2000 Mitutoyo hardness test machine. The depth-controlled indentation results were obtained under the constant loading/unloading rates of $0.025\ \text{N/s}$ with holding time of 5 s at maximum load. The electrochemical corrosion test was performed using conventional three electrodes solatron electrochemical testing system (1280B), with Ag/AgCl electrode as reference and platinum plate as the counter electrode. The sample was immersed as working electrode into 1 L of electrolyte solution containing 3.5 wt.% NaCl. The exposed surface area of tested specimen in solution was $1\ \text{cm}^2$. The polarization curves were recorded by increasing voltage against reference electrode from -3.5 to $2\ \text{V}$ at a scan rate of $1\ \text{mV/s}$. Corrosion potential and current was obtained using tafel analysis software, IVman package. All characterizations of the samples were carried out at room temperature.

3. Results and Discussions

3.1 Microstructure

Figure 1 shows the surface images of the coatings produced for different processing times. The coating surfaces are dominated by a ‘pancake’ shaped projections and channels with open or sealed microporosity in the center. Figure 1(a) shows the highest density of open pores at the centers of the ‘pancake’ structures. These micropores are considered to be the channels through which the Mg and Mg^{2+} from the substrate are ejected and reach the coating/electrolyte interface during the plasma-generated melting. It can be observed from the porosity relation with processing time in Fig. 3 that porosity decreases with increase in the processing time; however, at the same time, the pore size increases as shown in Fig. 1. The minimum porosity was obtained for 30-min processing time. From the SEM pictures, in addition to pores, several cracks and bumps can also be observed on the surface. The cracks size get enlarge with processing time. These micro cracks are caused from the thermal stress due to the rapid solidification of the molten oxide in the relatively cool electrolyte (Ref 30). However, they get magnify due to the increase in the tensile stress of the coating with increase in thickness. The surface image of 60-min sample shows less number of bulky pancakes with bigger sizes than any other coating. It is believed that due to the long processing time, these pancakes are unable to grow upward, rather sweep around, and mix along the boundaries.

Figure 2(a-d) shows the cross section morphologies of the coatings for different processing times. The sinus appearance of the interface is due to the nonuniform dissolution of substrate in the early phases of processing (Ref 20). Presence of inter-metallic phases such as α - and β -phase in AZ91D alloy has different corrosion affinity and thus causes nonuniform nucleation of the PEO layer. It can be observed, as marked in Fig. 2(b) that the discharge channels in the coatings cannot

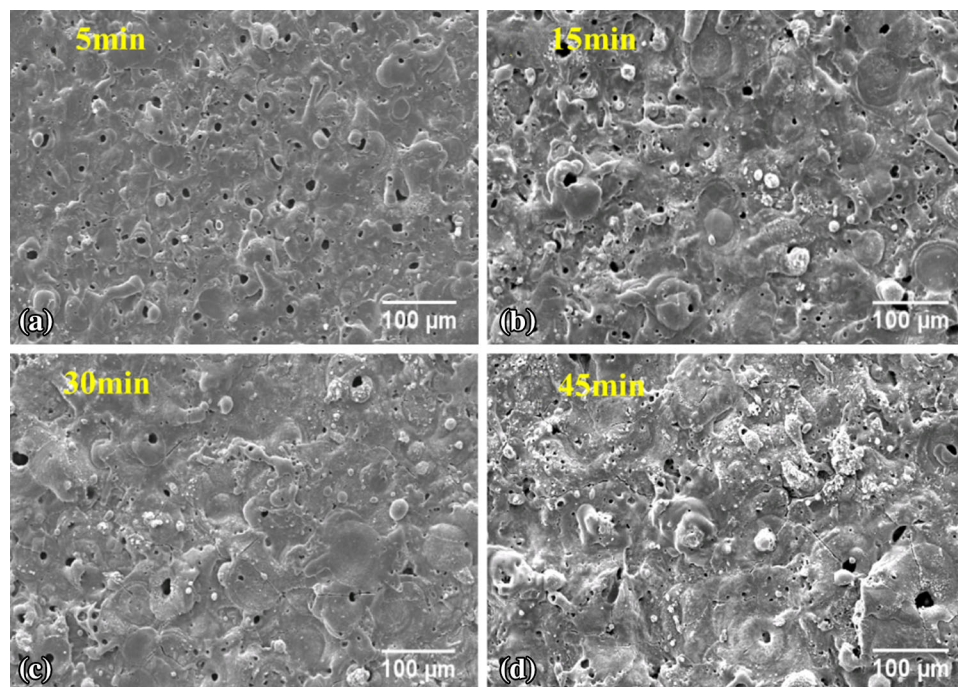


Fig. 1 Surface morphologies of PEO coated magnesium AZ91D alloy. (a = 5 min), (b = 15 min), (c = 30 min), (d = 60 min)

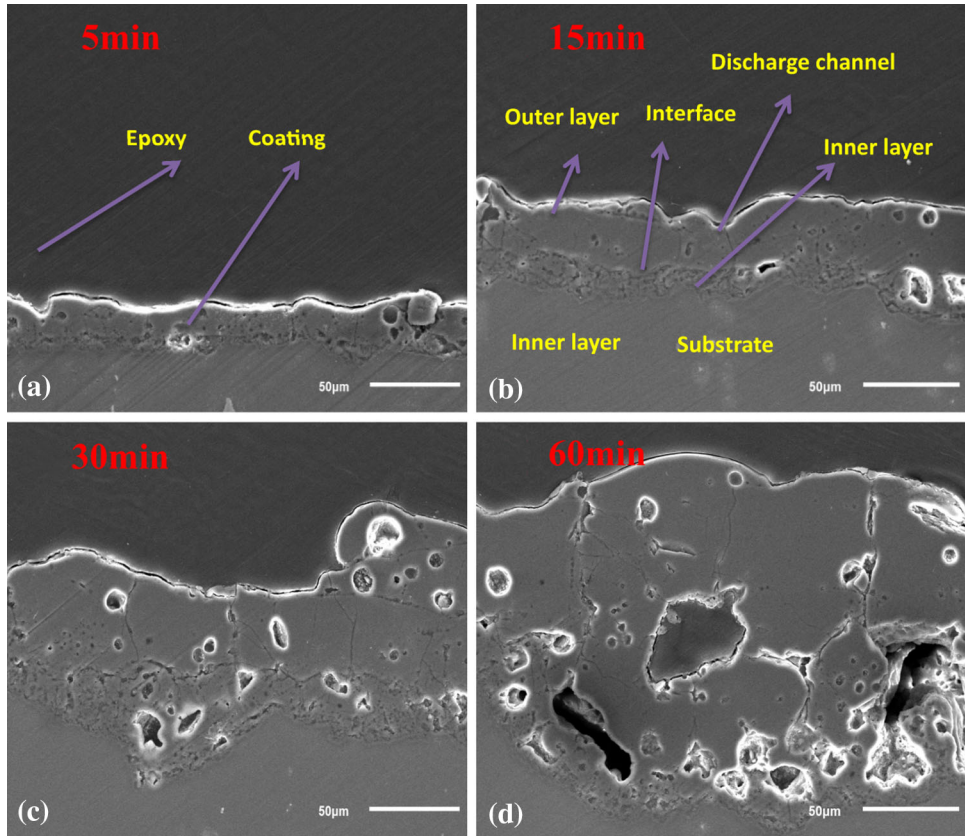


Fig. 2 Cross-section images of PEO coating on AZ91D alloy. (a = 5 min), (b = 15 min), (c = 30 min), (d = 60 min)

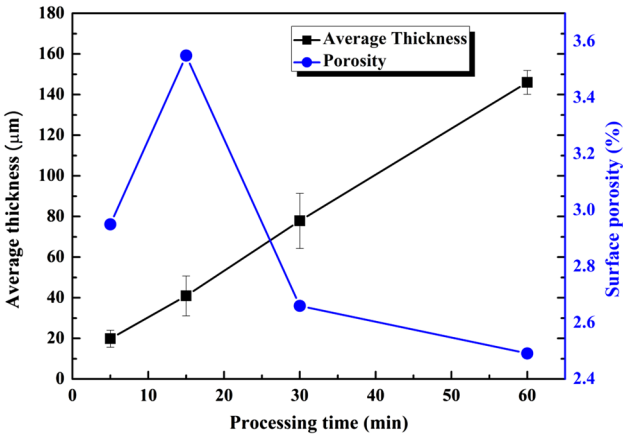


Fig. 3 Thickness and porosity of the coatings prepared for different processing time

penetrate through the whole thickness, however, end inside the layers at a certain depth from the surface of the coating. The depth where the discharge channels stop vary with processing time as shown in Fig. 2. For instance, the average D_d (discharge depth) for 5 and 15-min coatings was measured as 7.65 and 12.50 micron, respectively. The layer, where the discharge channels stops and cannot penetrate further is termed as an interface between the outer and inner layer. Above the interface layer, there exist outer layer which is dense and free of connected defects. However, the inner coating Fig. 2(a-d)

consists of significant amount of connected porosity. Average thickness of the coating is shown in Fig. 3. It can be observed that thickness increases linearly with processing time (Ref 31, 32). However, some authors observed the breakdown of linearity at longer treatment (Ref 33, 34). It is considered that fluorides play a catalytic role during PEO process, so the highest value of thickness achieved can be attributed to the long time treatment and use of Na_2SiF_6 in the electrolyte solution. Detail observation of the PEO coatings reveals that average thickness can be regarded as the sum of coating thickness above the original surface of the sample and below the original surface toward the magnesium alloy substrate.

3.2 Coating Composition and Phase Analysis

The relative amount of elements on the coating surface was examined by EDS and the results are listed in Table 1 and plotted in Fig. 4. It can be observed that all the coatings produced in the electrolyte (Na_2SiO_3 , NaOH , and Na_2SiF_6) are composed of Mg, Si, O, F, Al, and Na. Mg and Al contents participated in the PEO reactions as a substrate species, while the other elements contributed from electrolyte. Elements like O and F presents an increasing trend with processing time, while Si decreases. Variation of the elements with processing time suggests a change in ratio of chemical complexes with processing time. Notably, though Na is a cathodic component; however, it sticks to the coating and afterward mixed up in the coating due to very rapid plasma reactions. In Fig. 4, the element Au was supplied from the gold coatings on the sample for SEM analysis purposes.

Table 1 The relative contents of the main elements on the surface of the coatings by EDS analysis

Processing time (min)	Content of elements (at.%)					
	O	Mg	Si	F	Al	Na
5	49.93	28.20	16.77	0.23	2.42	2.36
15	51.83	27.51	15.22	0.43	2.51	2.50
30	51.74	28.05	14.54	0.67	2.47	2.35
60	53.26	25.14	14.25	0.92	2.18	4.06

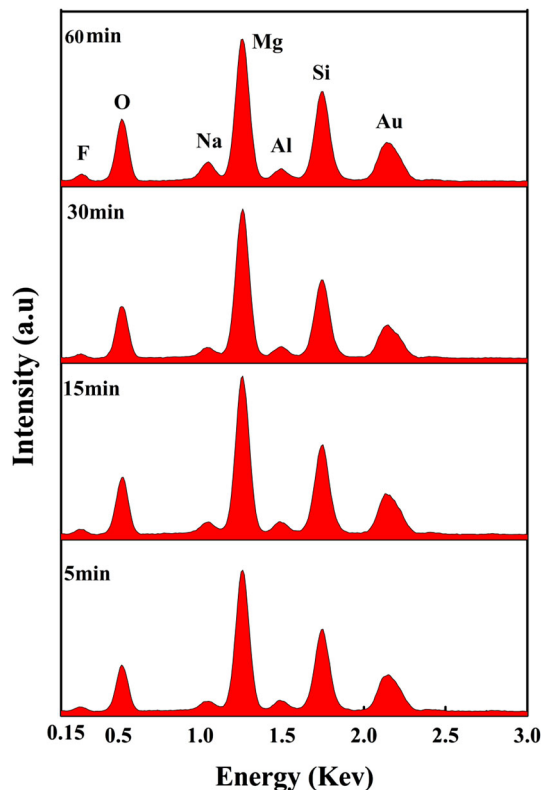


Fig. 4 EDS pattern of the PEO coating for different processing time

Figure 5 depicts the XRD pattern of the coatings prepared for different processing times. The phases in the pattern were identified as Mg_2SiO_4 , MgO , and MgF_2 . After comparing the XRD pattern with ICSD Reference code: 01-079-0612, it was found that all the peaks of cubic MgO were obtained in the pattern. Surprisingly, the relative intensities of MgO peaks (60 min) were quite similar to that of the reference. This suggests that crystallites of MgO are free of texture, which happens very rarely in the PEO process. The highest peak (200) of MgO lies at $2\theta = 42.8$ as seen in the Fig. 5. Moreover, beside MgO , orthorhombic Mg_2SiO_4 peaks were also identified in the pattern; however, due to complex reaction stages of silicates during PEO process, the relative intensities of Mg_2SiO_4 could not match with the reference. For instance, peak at $2\theta = 35.6$ is the second most intensive peak of the reported orthorhombic Mg_2SiO_4 phase; however, this did not happen in the experimental pattern. The difference in the relative intensities of the experimental and the reference pattern suggests a possible crystallographic texture in the Mg_2SiO_4 phase as well as justifying the presence of amorphous SiO_2 in

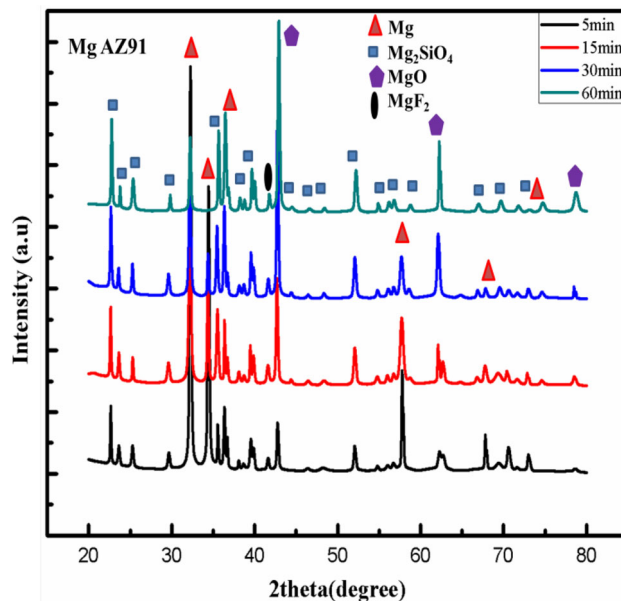


Fig. 5 XRD of the PEO coatings for different processing time

the coatings. Increase in the reaction time causes a significant increment in the relative intensities of all peaks in the pattern excluding the substrate. Furthermore, presence of significant proportion of amorphous material in the coating cannot be denied, as indicated by the high background at low angle, and broad peaks in the background trace at approximately 63° . In addition to other phases, peaks of crystalline MgF_2 were also observed in the XRD pattern. The presence of MgF_2 in the coating layer indicates that Na_2SiF_6 has participated in the reaction and after decomposition been incorporated into the oxide films. Presence of MgF_2 complies with the EDS result of detecting F on the surface of the coatings. MgF_2 have several promising effects such as upgrading the adhesion strength and corrosion resistance of the coating. As it is well known, the amount of each phase in the coating has very significant effects on the mechanical and corrosion properties of the coatings. Therefore, in order to determine the relative fraction of each phase, the coatings were characterized by considering the intensity of the main peaks of each phase in the XRD patterns. Figure 6 shows the ratio of the intensities and the relative variation of the MgO and Mg_2SiO_4 phases with processing time. It was found that the ratios of MgO to $Mg_2SiO_4 \sim I_{MgO}/I_{Mg_2SiO_4}$ are 0.83, 1.75, 2.4, and 2.3 for the coatings, produced for 5 min, 15 min, 30 min, and 60 min respectively. The results indicate increase in the ratio of MgO with processing times.

3.3 Hardness and Potentiodynamic Polarization

To study the mechanical properties of the coatings, average micro-hardness was measured for each coated specimen. It can be seen from Fig. 7 that hardness of the coatings was improved with increase in the processing time. The coating prepared for 60 min has the highest hardness value of (1271 HV ~13 GPa). Obviously, coating with such a high value can offer significant surface protection to the AZ91D alloy (~75 HV). The scatter in the hardness as can be inferred from the bars in Fig. 7 is supposed to be the result of amorphous material in the coatings together with porosity distribution. Moreover, the scatter in the hardness reflects the true hardness distribution of the coatings. Furthermore, it was revealed in many reports that hardness of the coating on AZ-series magnesium alloy is less than ~1000 HV. For instance, Yong Han et al. reported hardness ~1240 HV for $Mg_2Zr_5O_{12}/Mg_2Zr_5O_{12}-ZrO_2-MgF_2$ -based coatings produced at ~550 V on pure magnesium (Ref 35). Recently, salih durdu et al., obtained hardness of the inner layer ~1063HV, using the same experimental conditions except the use of Na_2SiF_6 in the electrolyte solution (Ref 20). It is therefore believed that the maximum value of the average hardness obtained in this work is due to the maximum thickness and the use of Na_2SiF_6 in the electrolyte solution that subsequently generated MgF_2 phase in the coating. It is worthy to mention that surface micro-hardness of substrate significantly helps improve the wear resistance. This can be understood from the following relationship which shows that wear rate has an inverse relation with hardness (Ref 36):

$$w = kL/H, \quad (\text{Eq 1})$$

where, w is the wear rate, k is the wear coefficient, L is the applied load, and H is the hardness of the material. Thus, it can be asserted that the coatings prepared for 60 min will surely have the highest wear resistance.

Figure 8 reveals the potentiodynamic polarization curves of the coated samples and AZ91 bare alloy. Tafel slopes were determined from these plots by curve fitting using IVman software package. Based on the ‘‘bestfit,’’ values of anodic and cathodic tafel slopes (β_a and β_c) and the corresponding values of corrosion potential (E_{corr}), polarization resistance (R_p), and corrosion current density (i_{corr}) were recorded as summarized in Table 2. However, due to the absence of tafel region on the

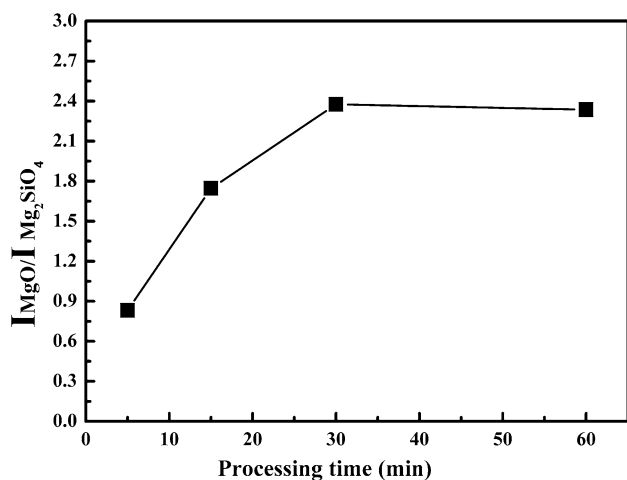


Fig. 6 Relative intensity ratio between MgO and Mg_2SiO_4 phases

anodic side for 5- and 15-min coatings, their corrosion currents were obtained from cathodic curves. It can be seen from Fig. 8 that the anodic and cathodic tafel slopes (β_a and β_c) of 5-min coating have large difference. However, the difference significantly decreases for 60-min-coated sample. The difference in the tafel slopes (β_a and β_c) arises due to the asymmetry of the cathodic and anodic reactions for short-time coatings. However, excellent symmetry can be observed for both parts of the polarization curve (anodic and cathodic) as the processing time approached to 60 min.

Generally, the cathodic polarization curve denotes the hydrogen evolution through water reduction, while the anodic polarization curve is attributed to the dissolution of AZ91 (Ref 37). As shown in Fig. 8, sample treated for 5 min has the highest value of the corrosion current; this is due to the low thickness and porous nature of coating, which allowed the corrosive solution to easily penetrate into the substrate. Moreover, the active region as denoted by the arrows in Fig. 8 extended very sharply for 5-min-coated sample and have reached a limiting current density of about 0.1 A/cm^2 , preceded by the pseudo-passive region formed by the diffusion and/or

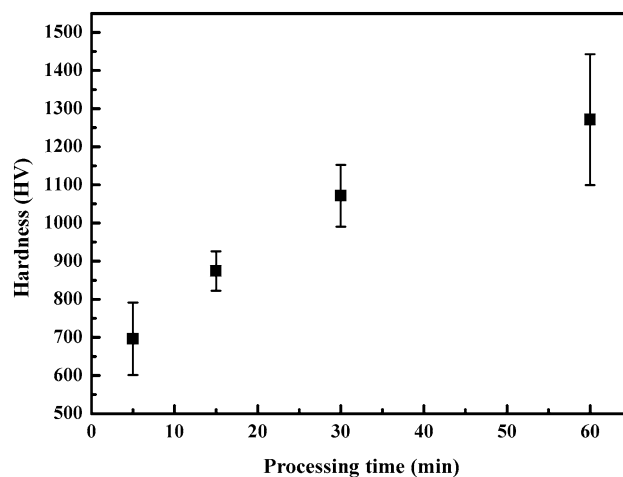


Fig. 7 Hardness of PEO coatings prepared on AZ91D alloy for different processing time

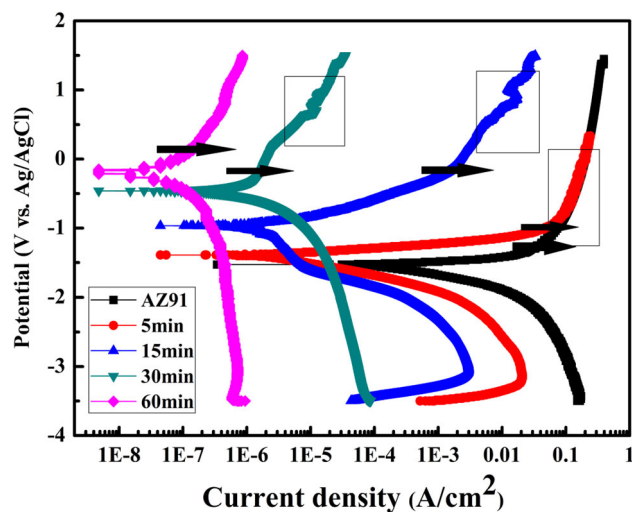
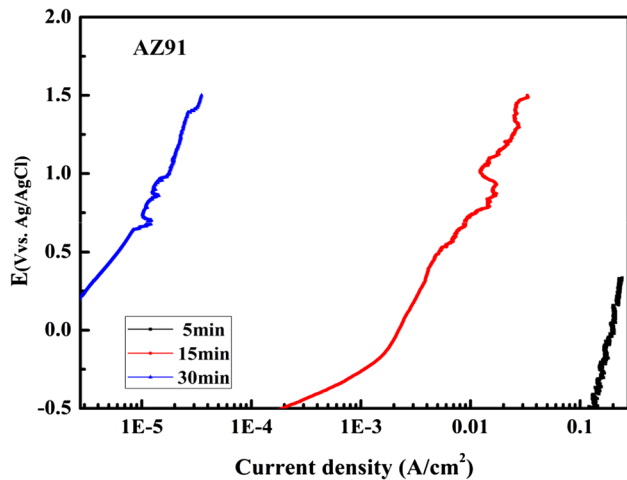


Fig. 8 Potentiodynamic polarization curves of the coated samples and bare AZ91 alloy

Table 2 Comparison of various potentiodynamic polarization results with this study

Ref.	Processing time (min)	Alloy	β_a (V/dec)	β_c (V/dec)	E_{corr} (V)	I_{corr} (A/cm ²)	Test medium
This study	...	AZ91	0.42	0.82	-1.5	5.00×10^{-3}	3.5 wt.% NaCl
	5	-1.36	4.02×10^{-4}	
	15	-0.95	2.38×10^{-5}	
	30	...	1.82	0.44	-0.44	1.04×10^{-6}	
60	...	0.90	0.82	-0.25	0.43×10^{-7}		
(Ref 24)	...	AZ91	-1.15	9.61×10^{-9}	3.5 wt.% NaCl

**Fig. 9** Zoom plot of the metastable pitting zone (encircled in Fig. 8)

dissolution of magnesium ions. The pseudo-passivation state in the 5-min sample is also accompanied by metastable pitting as can be observed from the noise in the current density (zoomed in Fig. 9). It is believed that the metastable pitting region arise from the breakdown of the corrosion product like Mg(OH)₂ and MgCl₂ that try to block the further inflow of corrosive solution. Contrary to the other samples, 60-min sample achieves the pseudo-passive state very quickly, indicating the efficient retardation of the corrosive ions by the coating. The sample treated for 60-min processing time has the highest value of corrosion resistance and lowest value of corrosion current recorded as 0.43×10^{-7} (A/cm²), comparable to the work reported by Young et al. (Ref 26). This can be attributed to the 60-min optimal PEO processing time, which promoted coating with fewer pores and cracks, larger thickness, and greater compactness as shown in Fig. 1(d), 2d, and 7 (Ref 28). The corrosion current of all the samples can be ranked as 60 min < 30 min < 15 min < 5 min < AZ91. Moreover, it is speculated that due the long processing time, amount of MgF₂ increases in the inner layer and hence bar the corrosive solution to reach the substrate more efficiently. Therefore, in addition to high thickness, the presence of MgF₂ phase seems to be a valid reason for such a high nobility of the 60-min coatings. For instance, M. Laleh et al., have performed the same kind of work for even longer processing time \sim 70 min, without the use of fluoride compound. Therefore, the obtained nobility ($E_c = -1.42$ V) was much lower than this study (Ref 23).

In addition to the general corrosion, a metastable pitting process also contributed during the polarization measurement. Pitting corrosion can occur when a local breakdown of the passive film takes place in an aqueous solution on a micro-

scopic scale (nucleation process). Pitting corrosion can be observed by the noisy portions on the tafel curves as can be seen in Fig. 9 (enclosed in Fig. 8). A decrease in the metastable pitting region was observed with processing time and surprisingly the metastable pitting zone was disappeared for 60-min processed specimen as can be seen in Fig. 8. Since the 60-min-coated sample is corroding with a very small current density above the corrosion potential to the overvoltage \sim 1.5 V. The negligible amount of current above the corrosion potential validate the highly obstructive behavior of the coating for the Cl⁻ ion to produce any significant amount of pits. Furthermore, stable pseudo-passivation state of the 60-min specimens without any metastable pitting zone verifies the superior quality of this coating.

4. Conclusions

PEO ceramic coatings were prepared on AZ91D in silicate-fluoride-based electrolyte. The results indicated that hardness and corrosion properties of the coatings were highly improved with processing time. The highest values of hardness \sim 1271.2 HV and corrosion potential \sim -0.25 V was obtained for the coating produced for 60-min processing time. The improved corrosion and hardness of the coatings can be attributed to two factors; first, due to the long time process time \sim 60 min, which made it possible to produce coatings with highest thickness \sim 147.12, and second, the use of Na₂SiF₆ in the electrolyte solution that contributed in the formation MgF₂ phase in the coating layer. It is therefore expected that the results obtained in this work could be utilized for further research work.

Acknowledgments

This work was supported by the National Research Foundation of Korea (NRF) grant funded by the Korea government (MSIP) (No. 2011-0030058) and (No. 2015R1A2A2A01007973).

References

1. E. Ghali, *Corrosion Resistance of Aluminium and Magnesium Alloys Understanding, Performance and Testing*, Wiley, New York, 2010
2. J. Liang, B. Guo, J. Tian, H. Liu, J. Zhou, and T. Xu, Effect of Potassium Fluoride in Electrolytic Solution on the Structure and Properties of Microarc Oxidation Coatings on Magnesium Alloy, *App. Surf. Sci.*, 2005, **252**(2), p 345–351
3. M. Avedesian and H. Baker, *ASM Speciality Handbook-Magnesium and Magnesium Alloys*, ASM International, Cleveland, 1999
4. G. Song and A. Atrens, Corrosion Mechanisms of Magnesium Alloys, *Adv. Eng. Mater.*, 1999, **1**(1), p 11–33

5. Shou-Ren Wang, Pei-Quan Guo, Li-Ying Yang, and Yanjun Wang, Microstructure and Mechanical Properties of AZ91 Alloys by Addition of Yttrium, *J. Mater. Eng. Perform.*, 2008, **2**, p 137–144
6. G.L. Maker and J. Kruger, Corrosion Studies of Rapidly Solidified Magnesium Alloys, *J. Electrochem. Soc.*, 1990, **137**(2), p 414–421
7. E. Aghion, B. Bronfin, and D. Elezer, The Role of the Magnesium Industry in Protecting the Environment, *J. Mater. Process. Technol.*, 2001, **117**(3), p 381–385
8. J. Zhou, Q. Li, H. Zhang, and F. Chen, Corrosion Behavior of AZ91D Magnesium Alloy in Three Different Physiological Environments, *J. Mater. Eng. Perform.*, 2014, **23**(1), p 181–186
9. R. Ambat, N.N. Aung, and W. Zhou, Evaluation of Microstructural Effects on the Corrosion Behaviour of AZ91D Magnesium Alloy, *Corros. Sci.*, 2000, **42**(8), p 1433–1455
10. G. Song, A. Atrens, D.S.T. John, X. Wu, and J. Nairn, Influence of Chloride Ion Concentration on Immersion Corrosion Behavior of Plasma Sprayed Alumina Coatings on AZ31B Magnesium Alloy, *J. Magnes. Alloys*, 2014, **2**(4), p 325–334
11. Y. Maoa, Z. Lia, K. Fenga, X. Guob, Z. Zhouc, and Y. Wu, Corrosion Behavior of Carbon Film Coated Magnesium Alloy with Electroless Plating Nickel Interlayer, *J. Mater. Process. Technol.*, 2015, **219**, p 42–47
12. R.O. Hussein, X. Nie, and D.O. Northwood, An Investigation of Ceramic Coating Growth Mechanisms in Plasma Electrolytic Oxidation (PEO) Processing, *Electrochim. Acta*, 2013, **112**, p 111–119
13. Z. Shi, G. Song, and A. Atrens, Influence of Anodising Current on the Corrosion Resistance of Anodised AZ91D Magnesium Alloy, *Corros. Sci.*, 2006, **48**(8), p 1939–1959
14. A. Ghasemi, V.S. Raja, C. Blawert, W. Dietzel, and K.U. Kainer, Study of the Structure and Corrosion Behavior of PEO Coatings on AM50 Magnesium Alloy by Electrochemical Impedance Spectroscopy, *Surf. Coat. Technol.*, 2008, **202**(15), p 3513–3518
15. A.L. Yerokhin, X. Nie, A. Leyland, A. Matthews, and J. Dowey, Plasma Electrolysis for Surface Engineering, *Surf. Coat. Technol.*, 1999, **122**(2), p 73–93
16. Y.L. Wang, W. Wang, M. Zhou, B.J. Li, G. Amoako, and Z.H. Jiang, Microstructure Characterization of Alumina Coating on Steel by PEO, *Surf. Eng.*, 2013, **29**(5), p 276–280
17. J. Curran, Plasma Electrolytic Oxidation for Surface Protection of Aluminium, Magnesium and Titanium Alloys, *Trans. IMF*, 2011, **89**(6), p 295–297
18. K.C. Tekin, U. Malayoglu, and S. Shrestha, Tribological Properties of Plasma Electrolytic Oxide Coatings on Magnesium Alloys, *Tribol. Mater. Surf. Interfaces*, 2012, **6**(2), p 67–74
19. R. Arrabal, E. Matykina, T. Hashimot, P. Skeldon, and G.E. Thompson, Characterization of AC PEO Coatings on Magnesium Alloys, *Surf. Coat. Technol.*, 2009, **203**(16), p 2207–2220
20. S. Durdu, S. Bayramoglu, A. Demirtas, M. Usta, and A.H. Ucisik, Characterization of AZ31 Mg Alloy Coated by Plasma Electrolytic Oxidation, *Vacuum*, 2013, **88**, p 130–133
21. Z. Yaoa, Y. Xua, Y. Liua, D. Wang, Z. Jianga, and F. Wang, Structure and Corrosion Resistance of ZrO₂ Ceramic Coatings on AZ91D Mg Alloys by Plasma Electrolytic Oxidation, *J. Alloys Compd.*, 2011, **509**, p 8469–8474
22. Z.P. Yao, D.L. Wang, Q.X. Xia, Y.J. Zhang, Z.H. Jiang, and F.P. Wang, Effect of PEO Power Modes on Structure and Corrosion Resistance of Ceramic Coatings on AZ91D Mg Alloy, *Surf. Eng.*, 2012, **28**(2), p 96–101
23. M. Laleh, F. Kargar, and A.S. Rouhaghdam, Investigation of Rare Earth Sealing of Porous Micro-Arc Oxidation Coating Formed on AZ91D Magnesium Alloy, *J. Rare. Earth.*, 2012, **30**(11), p 1293–1297
24. Y.G. Ko, K.M. Lee, B.U. Lee, and D.H. Shin, An Electrochemical Analysis of AZ91 Mg Alloy Processed by Plasma Electrolytic Oxidation Followed by Static Annealing, *J. Alloys Compd.*, 2011, **509S**, p S468–S472
25. K.C. Tekin, U. Malayoglu, and S. Shrestha, Electrochemical Behavior of Plasma Electrolytic Oxide Coatings on Rare Earth Element-containing Mg Alloys, *Surf. Coat. Technol.*, 2013, **236**, p 540–549
26. Y.G. Ko, E.S. Lee, and D.H. Shin, Influence of Voltage Waveform on Anodic Film of AZ91 Mg Alloy Via Plasma Electrolytic Oxidation Microstructural Characteristics and Electrochemical Responses, *J. Alloys Compd.*, 2014, **586**, p S357–S361
27. B.-H. Ahn, D.-G. Lee, H.-J. Cho, S.-R. Lee, F. Ahmed, M.S. Anwar, and B.-H. Koo, Effect of Na₂SiO₃ Concentration on the Properties of AZ31 Magnesium Alloy Prepared by Electrolytic Plasma Processing, *Electron. Mater. Lett.*, 2013, **9**(6), p 813–815
28. Y. Gao, A. Yerokhin, E. Parfenov, and A. Matthews, Application of Voltage Pulse Transient Analysis during Plasma Electrolytic Oxidation for Assessment of Characteristics and Corrosion Behaviour of Ca- and P-containing Coatings on Magnesium, *Electrochim. Acta*, 2014, **149**(19), p 3842–3850
29. Z.U. Rehman, B. Ahn, Y.S. Jeong, J. Song, and B. Koo, The Influence of Various Additives on the Properties of PEO Coatings Formed on AZ31 Mg Alloy, *Surf. Rev. Lett.*, 2016. doi:10.1142/S0218625X16500062
30. R.O. Hussein, D.O. Northwood, and X. Nie, The Influence of Pulse Timing and Current Mode on the Microstructure and Corrosion Behavior of a Plasma Electrolytic Oxidation (PEO) Coated AM60B Magnesium Alloy, *J. Alloys Compd.*, 2012, **54**, p 41–48
31. G. Sundararajan and L.R. Krishna, Mechanisms Underlying the Formation of Thick Alumina Coatings Through the MAO Coating Technology, *Surf. Coat. Technol.*, 2003, **167**(2), p 269–277
32. L.R. Krishna, L.R.C. Somaraju, and G. Sundararajan, The tribological Performance of Ultra-Hard Ceramic Composite Coatings Obtained Through Microarc Oxidation, *Surf. Coat. Technol.*, 2003, **163**, p 484–490
33. F. Mecuson, T. Czerwicz, T. Belmonte, T. Dujardin, A. Viola, and G. Henrion, Diagnostics of an Electrolytic Microarc Process for Aluminium Alloy Oxidation, *Surf. Coat. Technol.*, 2005, **200**(1), p 804–808
34. L. Chang, Growth Regularity of Ceramic Coating on Magnesium Alloy by Plasma Electrolytic Oxidation, *J. Alloys Compd.*, 2009, **468**(1-2), p 462–465
35. Y. Han and J. Song, Novel Mg₂Zr₅O₁₂/Mg₂Zr₅O₁₂-ZrO₂-MgF₂ Gradient Layer Coating on Magnesium Formed by Microarc Oxidation, *J. Am. Ceram. Soc.*, 2009, **92**, p 1813–1816
36. J.A. Williams, Wear Modelling: Analytical, Computational and Mapping: A Continuum Mechanics Approach, *Wear*, 1999, **225-229**(1), p 1–17
37. T. Lei, C. Ouyang, W. Tang, L.F. Li, and L.S. Zhou, Enhanced Corrosion Protection of MgO Coatings on Magnesium Alloy Deposited by An Anodic Electrodeposition Process, *Corros. Sci.*, 2010, **52**, p 3504–3508